minerals

MDPI

Article

Pyrite Characteristics and Its Environmental Significance in Marine Shale: A Case Study from the Upper Ordovician Wufeng–Lower Silurian Longmaxi Formation in the Southeast Sichuan Basin, SW China

Lei Chen [1,2,*], Xin Chen [1,2], Xiucheng Tan [1,2,3], Xuetao Hu [3] and Gaoxiang Wang [1,4]

[1] School of Geoscience and Technology, Southwest Petroleum University, Chengdu 610500, China; cx9306@126.com (X.C.); tanxiucheng70@163.com (X.T.); yuanyang0609@126.com (G.W.)
[2] Sichuan Natural Gas Geology Key Laboratory, School of Geoscience and Technology, Southwest Petroleum University, Chengdu 610500, China
[3] State Key Laboratory of Oil and Gas Reservoir Geology and Exploitation, School of Geoscience and Technology, Southwest Petroleum University, Chengdu 610500, China; axyx0612@163.com
[4] Research Institute of Shale Gas, Southwest Oil & Gas Field Company, PetroChina, Chengdu 610056, China
* Correspondence: cl211@126.com

Abstract: Pyrite, as a characteristic mineral in organic-rich marine shale, is a significant index for the interpretation of paleoredox conditions. In this study, based on drilling cores and focused ion beam-scanning electron microscopy (FIB-SEM), the occurrence, diameter and particle size distribution of pyrites from 32 samples obtained from the Wufeng–Longmaxi Formation in the southeast Sichuan Basin were analyzed. The results show that pyrite displays various occurrences at the macro-scale and micro-scale. At the macro-scale (mm–cm), pyrite laminations, nodular pyrites and lenticular pyrites can be found from drilling cores. At the micro-scale (nm–μm), the common occurrences of pyrite are pyrite framboids, euhedral pyrites and infilled pyrite framboids. According to the formation mechanism of pyrites, pyrites can be divided into syngenetic pyrites and diagenetic pyrites. The infilled pyrite framboids are categorized as diagenetic pyrites. The mean pyrite framboid diameters (Mean, D) range from 2.94 μm to 5.33 μm (average of 4.26 μm), with most samples showing pyrite framboid diameters from 3.5 μm to 4.8 μm. Most of the diameters of the framboid microcrystals (Mean, d) are less than 0.4 μm. Therefore, according to the (Mean, D) and the (Mean, d), the pyrite framboids can be divided into three sizes: syngenetic framboids (SF, D < 4.8 μm, d ≤ 0.4 μm), early diagenetic framboids (EDF, D > 4.8 μm, d > 0.4 μm) and late diagenetic framboids (LDF, D < 4.8 μm, d > 0.4 μm). Additionally, box-and-whisker charts of the diameter, standard deviation/skewness value of the mean diameter of pyrite framboids (Mean, D) and the ratio of trace elements indicate that the sedimentary water body was a euxinic–dysoxic environment. Euxinic conditions dominated the Wufeng Formation to the lower part of the Long11-3 section, which is beneficial for the preservation of organic matter. However, the middle-upper part of the Long13-Long12 sub-member is a dysoxic sedimentary environment.

Keywords: pyrite; marine shale; paleoredox condition; southeast Sichuan Basin; Longmaxi Formation

Citation: Chen, L.; Chen, X.; Tan, X.; Hu, X.; Wang, G. Pyrite Characteristics and Its Environmental Significance in Marine Shale: A Case Study from the Upper Ordovician Wufeng–Lower Silurian Longmaxi Formation in the Southeast Sichuan Basin, SW China. *Minerals* **2022**, *12*, 830. https://doi.org/10.3390/min12070830

Academic Editors: Rui Yang, Zhiye Gao, Yuguang Hou, Songtao Wu and Evgeny Galuskin

Received: 28 April 2022
Accepted: 27 June 2022
Published: 29 June 2022

1. Introduction

Sulfide of iron is an indispensable and particularly important component in the global biogeochemical cycle. In ancient sediments, sulfide of iron existed as the main form of pyrite. Sulfide of iron is also a major indicator for the interpretation of paleoredox conditions, so the formation of pyrite in sediments is the key to understanding the ancient environment in geological history [1], which is attracting more and more scientists to research pyrite [2–6]. The formation of pyrite is determined only by the microenvironment, so the fabric characteristics and the occurrence of pyrite assemblages inherited and retained

certain characteristics that formed during the sedimentation stage [7]. In sediments or sedimentary rocks, pyrite occurred in the form of (1) irregular assemblages, (2) framboids and (3) idiomorphic crystals. Pyrite framboids are formed by a large number of pyrite microcrystals with the same size (diameter generally ranging from 0.1 to 1 μm) and consistent morphology. The average diameter of a pyrite framboid is usually 5 μm, and very few pyrite framboids can reach up to more than 50 μm [8–10]. More and more researchers have pointed out that the diameter of a pyrite framboid is a reliable index for the interpretation of paleoredox conditions [11–17]. Normally, the maximum diameter of a pyrite framboid formed in the oxidized marine environment is larger than that formed in the reducing environment [11,18].

With the success of shale gas exploration in the southeast Sichuan Basin, more and more geologists are trying to study the favorable sedimentary environment that led to organic-rich marine shale in the Wufeng Formation–Longmaxi Formation [19–21]. Many of them used geochemistry data and some geochemistry indexes (e.g., U/Th and Ni/Co) to study paleoredox conditions during the Late Ordovician to the Early Silurian period in the southeast Sichuan Basin [22–26]. However, due to geochemical parameters, controlled by a variety of geological factors and influenced by human measurement and experimental equipment, it is not reliable to use a geochemical index to interpret paleoredox conditions.

In recent years, David Rickard's research has shown that the use of framboid size measurements as an index for the judgment of ancient sedimentary environments is basically valid, but it is not statistically reliable [27]. Therefore, we need to distinguish syngenetic pyrite from diagenetic pyrite. Research shows that the geometric mean diameter of modern syngenetic framboids formed within euxinic water columns is 4.7 μm, and that of diagenetic framboids formed within sediments is 6.7 μm [27]. Due to the deep burial stage, the diameter of diagenetic framboids that formed is similar to that of syngenetic framboids. However, syngenetic framboid microcrystal diameters are mainly distributed between 0.3 and 0.4 μm, and diagenetic framboid microcrystal diameters are larger than 0.4 μm [6].

According to the pyrite framboid diameter (D) and the framboid microcrystal diameter (d), pyrite framboids can be divided into three types: syngenetic framboids ($D < 4.7$ μm, $d \leq 0.4$ μm), early diagenetic framboids ($D > 4.7$ μm, $d > 0.4$ μm) and late diagenetic framboids ($D < 4.7$ μm, $d > 0.4$ μm) [6,27].

In this study, we used the maximum framboid diameter (MDF), pyrite framboid diameter, framboid microcrystal diameter and geochemistry index to interpret the sedimentary environment of organic-rich shale in the Wufeng Formation–Longmaxi Formation in the southeast Sichuan Basin. In this way, we can accurately judge the sedimentary environment of Longmaxi Formation shale with pyrite, where the sedimentary environment is closely related to the development of high-quality shale, in order to provide some guidance for the exploration and development of shale gas.

2. Geological Setting

The Upper Ordovician Wufeng–Lower Silurian Longmaxi marine shale, characterized by black carbonaceous shale and siliceous shale, is widely distributed in the Sichuan Basin and its surrounding area, with thicknesses ranging from 50 to 200 m [22,28–30]. The Upper Ordovician Wufeng–Lower Silurian Longmaxi marine shale shows a wide distribution, high TOC, great thickness, appropriate burial depth and high maturity [29,31–35], resulting in the Wufeng–Longmaxi shale as the main shale gas exploration target interval in the southeast Sichuan Basin.

The Lower Silurian Longmaxi Formation comprises a set of thin siliceous and carbonaceous shale and yields abundant *Graptolite* [36–39]. The thickness of organic-rich black shale in the Wufeng–Longmaxi Formation is generally 20–40 m in the southern Sichuan Basin. The Longmaxi Formation is divided into two members: the Long1 Member and Long2 Member. The Long1 Member is subdivided into two sub-members: Long11 and Long12. As the main commercial shale gas interval, the Long11 sub-member is further divided into four sections: Long11-1, Long11-2, Long11-3 and Long11-4 (Figure 1). In this

study, the Wufeng Formation to the Long11 sub-member of X and JY1 wells in the Fuling area was chosen as the research target.

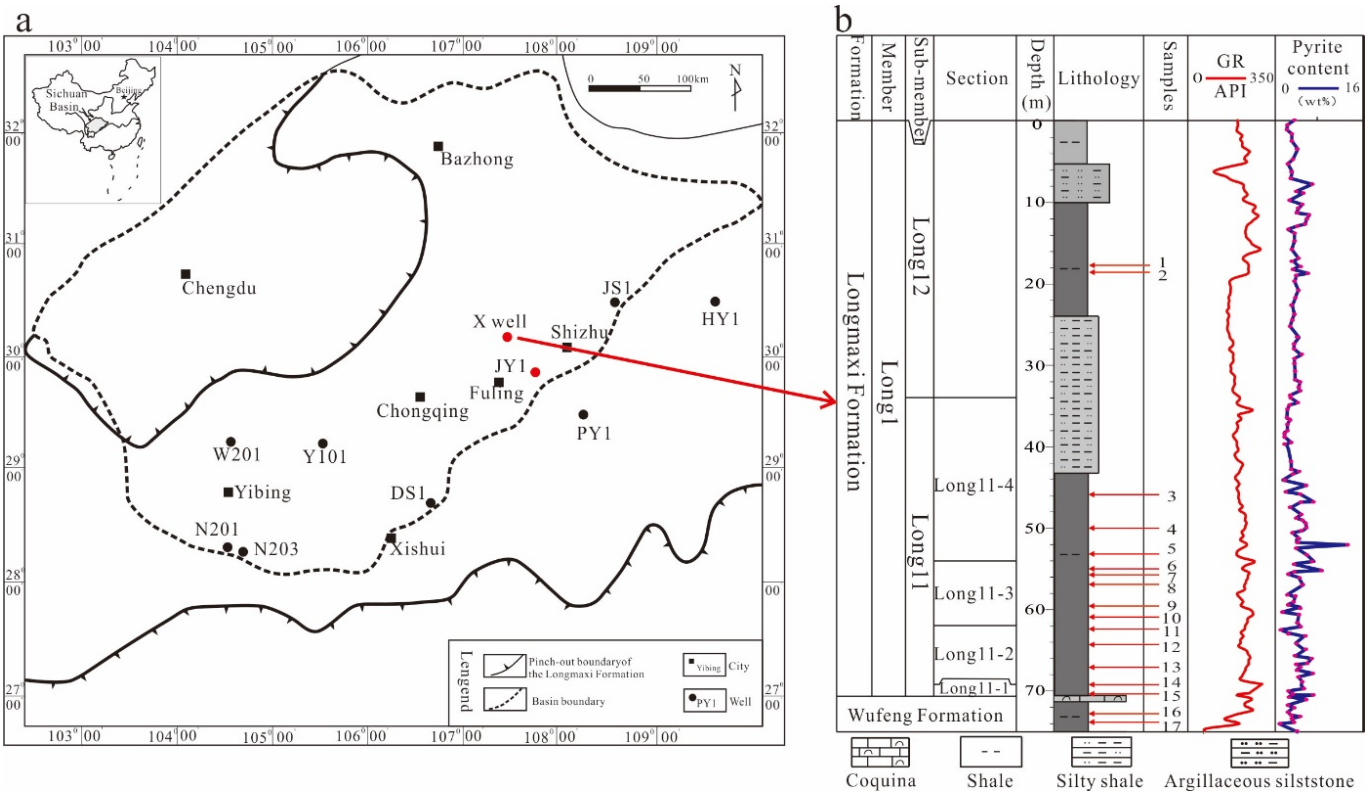

Figure 1. (**a**) Well location [22]. (**b**) The stratigraphic framework for the Upper Ordovician Wufeng Formation to the Lower Silurian Longmaxi Formation and the sampling location of the X well in the southeast Sichuan Basin.

3. Materials and Methods

In order to study the characteristics of pyrite and its environmental significance in the marine shale, two shale gas wells (X and JY1 wells) were selected in Southeast Sichuan. A series of analytical tests and experiments were carried out successively, including XRD whole-rock analysis, sub-ion polishing scanning electron microscopy, trace elements, etc. The specific test methods are as follows.

For trace element analysis, this study used the following method: (1) Accurately weigh 50 ± 1 mg of powder sample and place it in a Teflon crucible; (2) Wet the sample with 1–2 drops of high-purity water, and then add 1 mL of HNO_3 and 1 mL of HF in turn; (3) Put the Teflon crucible into the steel sleeve, tighten it, put it into the oven and heat it at 190 ± 5 °C for more than 48 h; (4) After the sample dissolution cools, put it on the electric heating plate (115 °C) and evaporate to dry, and then add 1 mL of HNO_3 and evaporate again (ensure that the Teflon crucible wall is free of liquid) (if there is a black suspended substance, add 1–2 drops of $HClO_4$ and evaporate to dry again); (5) Add 3 mL of 30% HNO_3 into the Teflon crucible, put the Teflon crucible into the steel sleeve again, tighten it and place it in the oven at 190 ± 5 °C, heating it for more than 12 h; (6) Transfer the solution to a polyethylene bottle, dilute it to 100 g with 2% HNO_3 and store it tightly for the ICP-TOF-MS test.

Sample preparation: 17 and 15 shale samples were taken from the Upper Ordovician Wufeng Formation to the Long1 section of well X and well JY1, respectively, and the selected samples were molded into 1 cm × 1 cm standard samples (Figure 1). Then, an IB-09010cp-type ion section polishing instrument was used to polish the sample surface with argon ion polishing technology, and a JSM-6700F-type cold field-emission scanning electron microscope was used to perform image acquisition under the conditions of 10 kV

accelerating voltage and 10 μA beam current. Finally, the pyrite framboid diameter of each sample was measured through the SEM image by using Image J (Table 1). This experiment was completed in the State Key Laboratory of Biochemical Engineering, Institute of Process Research, Chinese Academy of Sciences, Beijing, China.

Table 1. Descriptive statistics of pyrite framboid size distribution from the Wufeng and Longmaxi shales in the southeast Sichuan Basin.

Well	Formation	Sample ID	Depth (m)	Mean, D (μm)	Mean, d (μm)	Median Diameter (μm)	Maximum Diameter (μm)	Standard Deviation	Skewness	Framboids Measured
X	Long12	1	17.34	3.65	0.37	3.42	9.48	1.38	1.97	90
		2	18.21	4.01	0.4	3.5	8.37	1.55	1.33	86
	Long11-4	3	45.91	3.62	0.39	3.49	5.45	0.92	0.08	76
		4	49.99	3.57	0.37	3.33	9.86	1.22	1.68	147
		5	53.17	5.1	0.52	4.04	13.31	2.27	3.64	96
		6	55.05	5.32	0.61	4.1	16.27	1.96	3.86	69
	Long11-3	7	55.80	3.64	0.38	3.37	6.55	1.18	0.58	70
		8	56.63	3.71	0.36	3.38	8.69	1.43	1.23	64
		9	59.72	3.89	0.35	3.57	6.80	1.11	0.94	88
		10	60.93	4.32	0.37	3.75	10.91	1.99	1.75	54
	Long11-2	11	62.28	2.94	0.38	2.63	5.02	0.77	1.36	26
		12	64.17	4.35	0.41	3.75	13.69	1.82	2.21	62
		13	67.06	4.19	0.39	3.72	7.81	1.37	0.76	114
	Long11-1	14	69.11	4.1	0.41	3.93	8.19	1.04	1.32	141
		15	70.38	4.4	0.36	3.84	11.30	1.89	2.01	20
	Wufeng	16	72.78	4.65	0.39	4.31	15.53	1.96	2.34	285
		17	73.82	4.79	0.37	4.65	8.15	1.12	1.3	30
JY1	Long12	1	2330.46	5.33	0.55	4.18	14.28	1.89	2.84	148
		2	2335.30	4.37	0.38	3.39	7.79	1.68	1.8	72
		3	2340.82	4.82	0.48	3.62	12.27	2.06	3.7	88
		4	2346.50	5.08	0.51	3.31	11.90	1.98	3.32	165
		5	2352.89	4.4	0.35	4.32	9.97	1.57	1.06	125
		6	2359.98	4.36	0.36	4.17	9.75	1.43	1.18	102
		7	2366.74	4.82	0.45	4.14	6.90	2.13	2.54	69
		8	2376.05	5.17	0.49	3.74	8.85	2.41	2.96	99
	Long11-4	9	2381.91	3.76	0.38	3.54	7.52	1.16	0.93	146
		10	2385.42	3.83	0.35	3.74	9.05	1.31	1.22	121
	Long11-3	11	2391.95	4.92	0.46	3.51	8.47	2.09	3.25	95
		12	2397.13	3.96	0.37	3.79	6.57	1.06	0.43	90
	Long11-2	13	2402.55	3.67	0.37	3.50	7.12	1.13	0.75	117
		14	2406.16	3.83	0.39	3.50	7.12	1.13	0.74	110
	Long11-1	15	2411.05	3.89	0.36	3.85	9.27	1.54	1.33	75

4. Results and Discussion

4.1. Occurrence of Pyrite (Morphology of Pyrite)

Pyrite is widely developed in Longmaxi and Wufeng marine shale with various shapes in the Sichuan Basin [6,40], and the pyrite content is generally between 1% and 6%, with an average content of more than 2% [26,41,42].

In the drilling cores, various occurrences can be observed in the Upper Ordovician Wufeng to the Lower Silurian Longmaxi marine shale. Meanwhile, the pyrites are not disorderly and irregularly distributed in the shales. The pyrite mainly shows the following occurrences: (1) distributed in the form of lamination with a thickness ranging from 0.5 cm to 3 cm (Figure 2a,c,d); (2) lenticular pyrite developed within pyrite laminations (Figure 2c); (3) lenticular (Figure 2e) or pyrite nodules discontinuously distributed with a nodule size ranging from 0.5 cm × 2 cm to 1 cm × 3 cm (Figure 2d); and (4) scattered as fine-grain particles (Figure 2f).

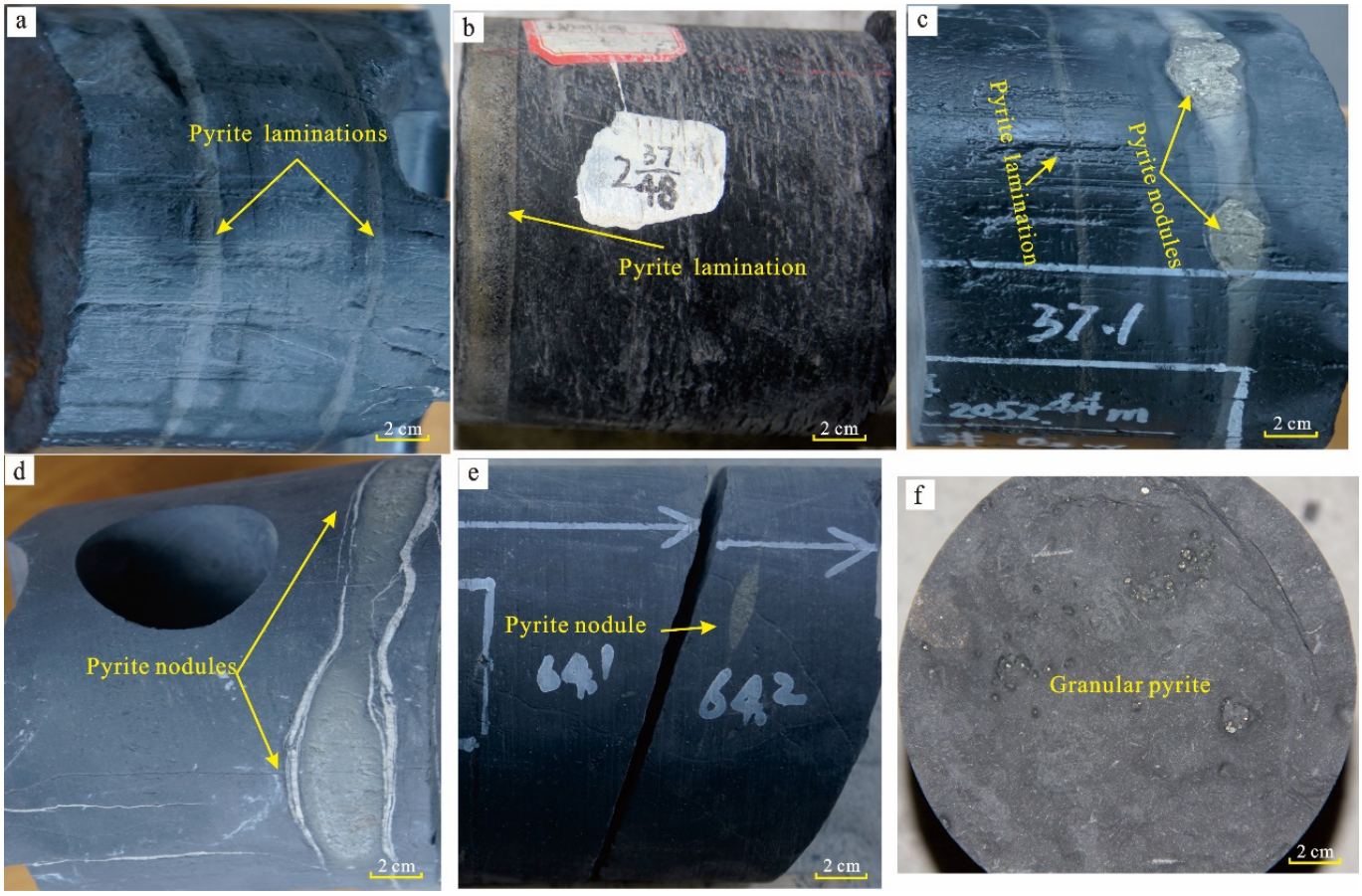

Figure 2. Macroscopical occurrence of pyrite in the Upper Ordovician Wufeng–Lower Silurian Longmaxi Formation. (**a**) Pyrite lamination in the Wufeng black shales, 72.40 m, X well. (**b**) Pyrite lamination in the gray silty shale of the Longmaxi Formation, 2338.6 m, JY1 well. (**c**) Lenticular pyrite developed within pyrite laminations in the Wufeng black shales, 70.44 m, X well. (**d**) Pyrite nodules show discontinuous distribution, 72.53 m, X well. (**e**) Pyrite nodules developed in the black silty shale of the Longmaxi Formation, 57.48 m, X well. (**f**) Pyrite lamination in the black carbonaceous shale of the Longmaxi Formation, 2355.8 m, JY1 well.

In the FIB-SEM image, the pyrite in the Wufeng–Longmaxi Formation shows the following occurrences and textures: pyrite framboids, subhedral–euhedral pyrites and infilled framboids. (1) Normal spherical pyrite framboids. These kinds of pyrite framboids show spherical or ellipsoid forms with diameters ranging from 3 μm to 12 μm. The maximum diameter of framboids can reach up to 17 μm. The pyrite framboids are mainly composed of euhedral pyrite microcrystals with a uniform size (0.1 μm to 1 μm). Abundant intercrystal nanopores can be found in normal spherical pyrite framboids (Figure 3a). The pyrite framboids can be divided into four types: syngenetic framboids (SF, D < 4.8 μm, d ≤ 0.4 μm) developed in the organic matter enrichment area (Figure 3a,d), early diagenetic framboids (EDF, D > 4.8 μm, d > 0.4 μm) (Figure 3a,d,e), late diagenetic framboids (LDF, D < 4.8 μm, d > 0.4 μm) (Figure 3a) and infilled pyrite framboids (IPF) categorized as diagenetic pyrites with poorly developed intercrystal nanopores (Figure 3a,b). (2) Subhedral–euhedral pyrites (S-EP) (Figure 3b,d,e). (3) Clustered pyrite framboids (CPF). These clustered framboids consist of abundant normal pyrite framboids, with each pyrite framboid's diameter ranging from 3 μm to 5 μm (Figure 3c). (4) Irregular aggregation of pyrite microcrystals (IAPM) (Figure 3e). (5) Aggregation of pyrite microcrystals (APM). Abundant pyrite microcrystals were packed to form an aggregation of pyrite with abundant intercrystal nanopores developed (Figure 3a,d,e).

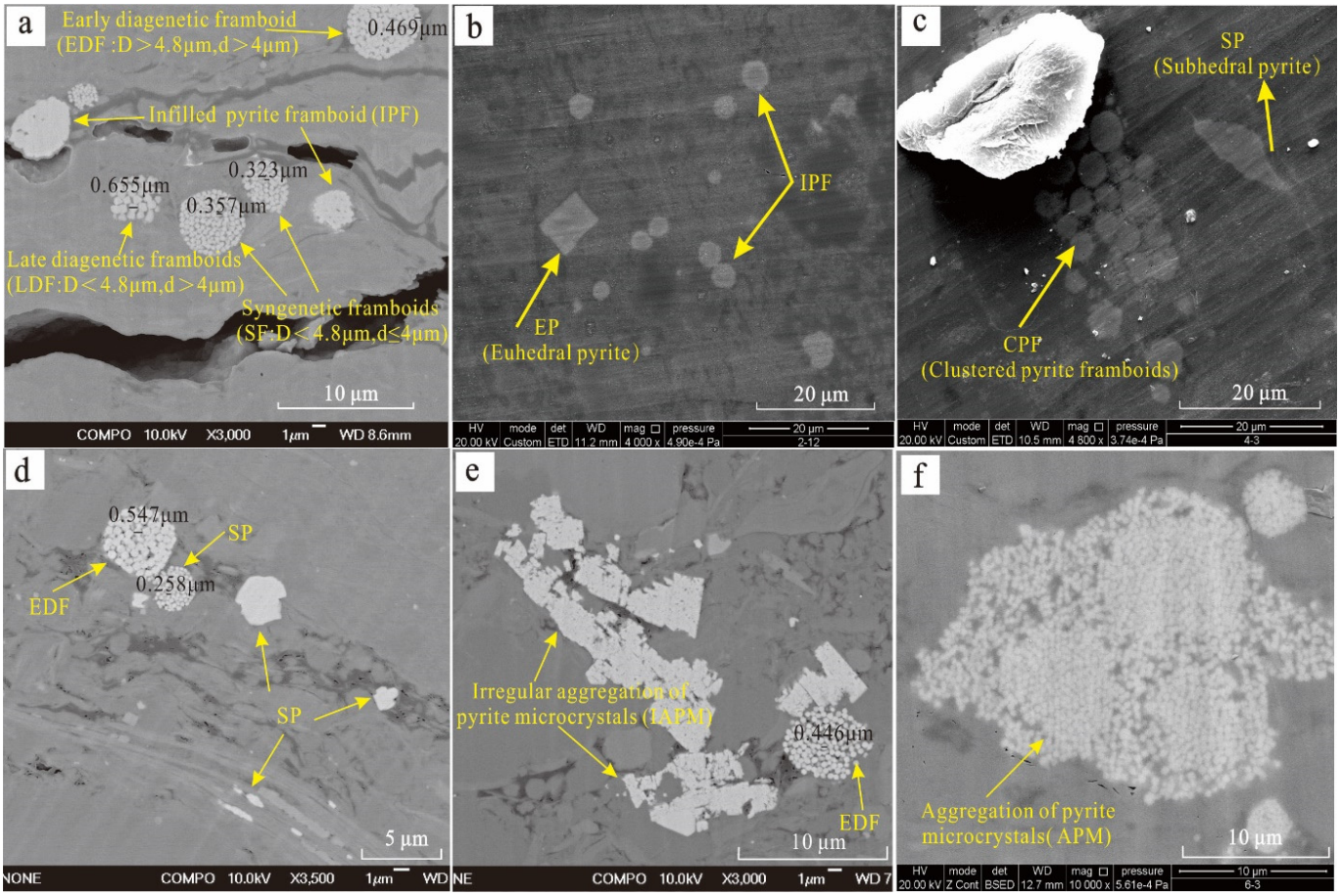

Figure 3. Pyrite micromorphology in the Longmaxi and Wufeng Formations. (**a**) Syngenetic framboids (SF), early diagenetic framboids (EDF), late diagenetic framboids (LDF) and infilled pyrite framboids (IPF) in the Longmaxi silty shale, 2330.46 m, well JY1; (**b**) infilled pyrites framboids (IPF) and euhedral pyrites (EP) in the Longmaxi black silty shale, 17.43 m, well X; (**c**) euhedral pyrites (EP) and clustered pyrite framboids (CPF) in the Longmaxi black silty shale, 45.91 m, well X; (**d**) syngenetic framboids (SF), early diagenetic framboids (EDF) and euhedral pyrites (EP) in Longmaxi black-gray silty shale, 2346.5 m, well JY1; (**e**) early diagenetic framboid (EDF) and irregular aggregation of pyrite microcrystals (IAPM) in the Longmaxi shale, 2397.13 m, well JY1; (**f**) aggregation of pyrite microcrystals (APM) in the Wufeng black shale, 72.78 m, well X.

An abundant occurrence of pyrite can be found in the Wufeng–Longmaxi Formation in the southeast Sichuan Basin, SW China. However, SEM analysis shows that the pyrites in the Wufeng–Longmaxi shales mainly exhibit three types of pyrites: pyrite framboids, subhedral–euhedral pyrites and infilled framboids.

4.2. The Size Distribution of Framboids and Microcrystals

As shown in Figure 4a, the main peak of the diameter of pyrite framboids ranges from 2.4 μm to 4.8 μm, accounting for 63.07% of the total. Thus, the size of the syngenetic pyrite framboids is suggested to be less than 4.8 μm, and the diagenetic pyrite framboids are larger than 4.8 μm [6,27]. As shown in Figure 4b, most of the diameters of the framboid microcrystals are less than 0.4 μm. Therefore, the size of the syngenetic framboid microcrystals is suggested to be less than 0.4 μm, and the diagenetic framboid microcrystals are larger than 0.4 μm [6].

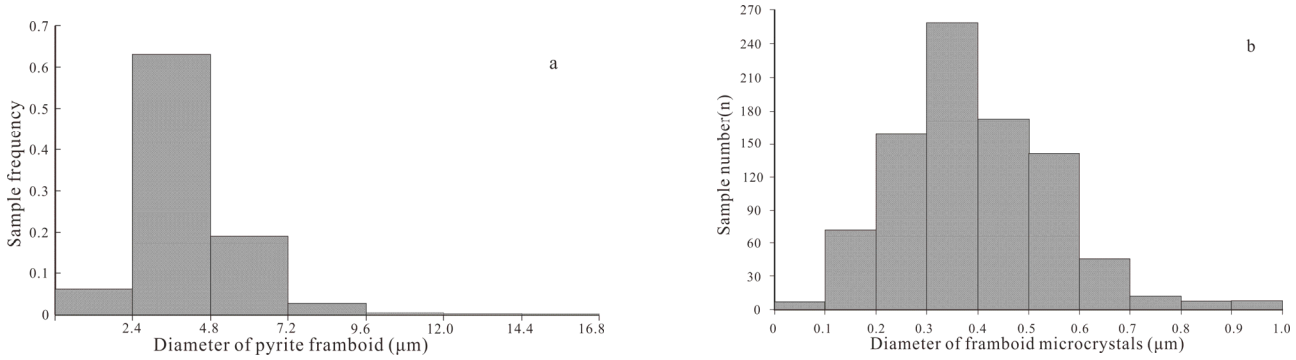

Figure 4. (**a**) Distribution of the diameter of pyrite framboids in the Wufeng and Longmaxi Formations; (**b**) Distribution of the diameter of framboid microcrystals in the Wufeng and Longmaxi Formations.

According to the morphological characteristics of pyrite in the Wufeng and Longmaxi shales (Table 1), the mean pyrite framboid diameters (Mean, D) of 32 samples range from 2.94 μm to 5.33 μm (average of 4.26 μm), with most samples showing pyrite framboid diameters from 3.5 μm to 4.8 μm, and more than 75% of pyrite framboids in black shales or black carbonaceous shales are smaller than 4.8 μm in mean size. Only a small number of pyrite framboids have a mean size larger than 4.8 μm in the Longmaxi black-gray silty shales and gray silty shales. The mean diameters of the microcrystals of the framboids (Mean, d) range from 0.35 μm to 0.61 μm (average of 0.41 μm). The median pyrite framboid diameters of all samples range from 2.63 μm to 4.65 μm, and the maximum pyrite framboid diameters of samples are in the range between 5.02 μm and 16.27 μm, mainly concentrated in the range from 5 μm to 10 μm (Table 1). The statistics of the size distribution, such as standard deviation and skewness, were calculated for 32 samples in the Wufeng–Longmaxi Formations. The variations in the standard deviation and skewness range from 0.77 to 2.41 and 0.08 to 3.86, respectively, with averages of 1.55 and 1.76, respectively. The average values of the standard deviation, skewness and (Mean, D) of the Long12 pyrite framboids (1.74, 2.19 and 4.53 μm) are higher than those of the Wufeng-Long11 pyrite framboids (1.47, 1.59 and 4.16 μm), which indicates that the pyrite framboids of the Long12 shales are more diverse and are larger than those of the Wufeng-Long11 shales (Table 1).

4.3. Paleoredox Condition Interpretation

Wilkin et al. (1996) [11] found that the particle size of pyrite framboids was determined in the early consolidation under anoxic conditions and was preserved in the later diagenetic solidification, meaning that the particle size of pyrite framboids would not have changed during the late diagenesis process. The particle size distribution of pyrite framboids in the drilling core samples or outcrop samples presents the original characteristics of the pyrite framboids. Therefore, the particle size distribution of pyrite framboids in ancient sediments can provide a reliable indication for interpreting paleoredox conditions [9].

Wignall and Newton (1998) [18] proposed using the maximum diameter of framboids (MDF) to distinguish between anoxic and oxic environments. Normally, the MDF of pyrite framboids that formed in an oxic environment is larger than that formed in an anoxic environment. Generally, 20 μm is a threshold value indicating where the paleoredox environment changed from an anoxic environment to a dysoxic–oxic environment [8]. The MDFs of pyrite framboids from the 32 samples are all less than 20 μm, mainly concentrated between 5~10 μm. Among these 32 samples, the MDFs of pyrite framboids from 9 samples (X well nos. 5, 6, 10, 12, 15 and 16 and JY1 well nos. 1, 3 and 4) are more than 10 μm, with the maximum value reaching 16.27 μm (Table 1, Figure 5). The MDFs of pyrite framboids from the X and JY1 wells indicate that the Wufeng Formation-Long12 was basically deposited in an anoxic environment.

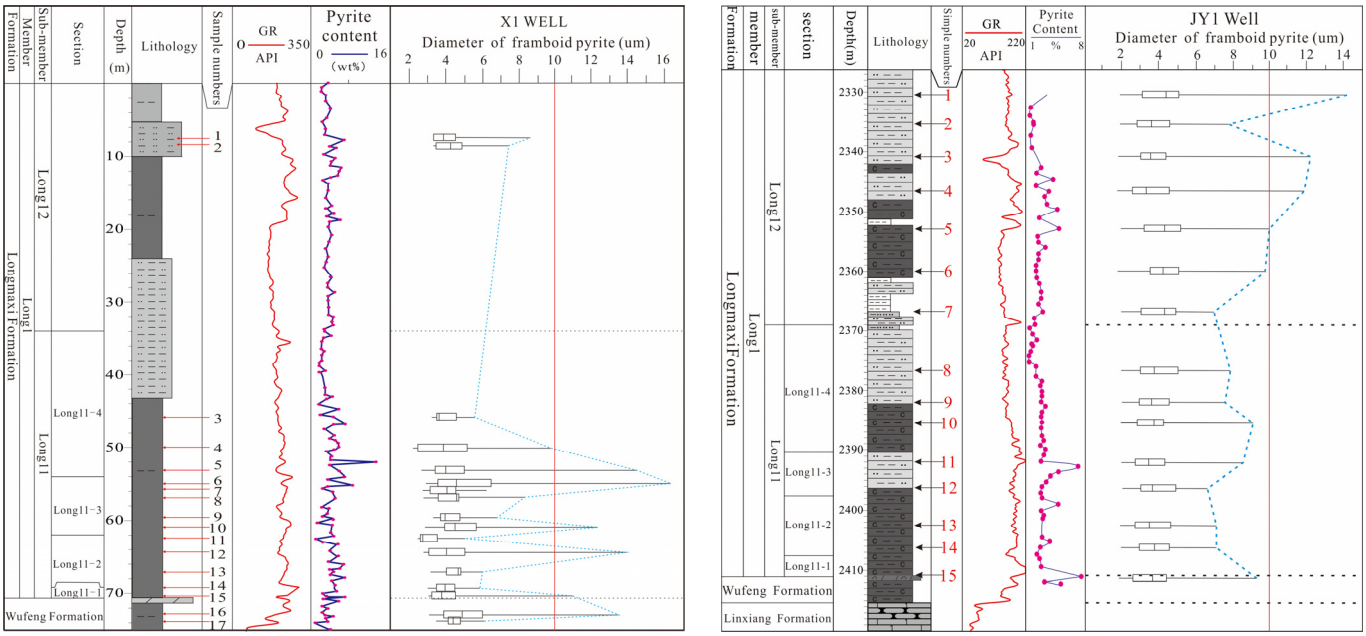

Figure 5. (**a**) Logs of the Wufeng–Longmaxi Formation from the X well pyrite framboids represented as "box-and-whisker" plots, where the "box" depicts the 25th and 75th percentiles of framboid distributions, the "whiskers" depict the minimum and maximum framboid diameters, and the central line is the median average. (**b**) Logs of the Wufeng–Longmaxi Formation from the JY1 well pyrite framboids represented as "box-and-whisker" plots, where the "box" depicts the 25th and 75th percentiles of framboid distributions, the "whiskers" depict the minimum and maximum framboid diameters, and the central line is the median average.

Most of the samples show mean pyrite framboid diameters (Mean, D) less than 5 μm, ranging from 2.94 μm to 4.92 μm (Table 1). Wilkin et al. (1996) [11], Bond and Wignall (2010) [43] and Wignall et al. (2010) [44] believed that when anoxic conditions dominated the sedimentary environment, a large number of pyrite framboids with small diameters (3~5 μm) would have formed. In suboxic conditions (weakly oxygenated in bottom waters), the average diameter of framboid pyrites can reach more than 6 to 10 μm (Wilkin et al., 1996; Bond and Wignall, 2010) [11,43]. The mean pyrite framboid diameters (Mean, D) from the Wufeng-Long12 shale show that anoxic conditions dominated the environment during the shale depositional process.

The box-and-whisker plots illustrate that the framboid size significantly changes several times from the bottom to the top, which may indicate that the study area underwent several environmental changes from anoxic to suboxic conditions during the Longmaxi marine shale depositional process (Figure 5).

The size-frequency distributions of framboids show that 85% of pyrite framboids from all samples have a small size (less than 4.8 μm) (Figure 4a). Only a few pyrite framboids show a large size (>10 μm). The dominant size of framboids in each stratum (Wufeng-Long12) is between 2.4 μm and 4.8 μm, indicating that the water column was dominated by anoxic conditions from the Wufeng Formation to the Long12.

Based on the standard deviation and skewness, pyrite framboids from euxinic and oxic-dysoxic environments are plotted (Figure 6a,b). Most of the samples drop in the area of euxinic environments, except for some samples that occur in dysoxic environments (Figure 6a,b).

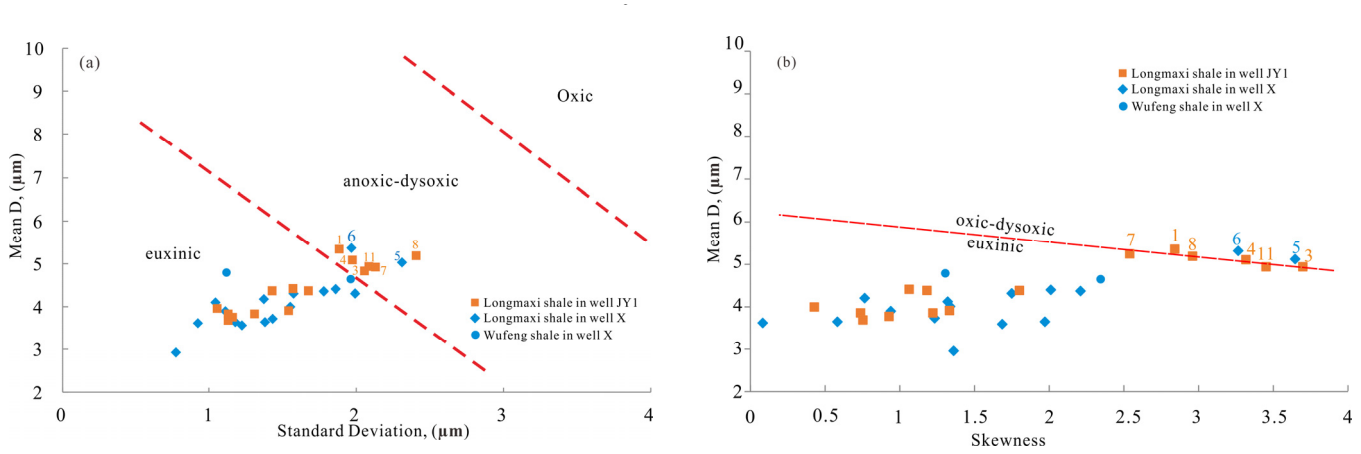

Figure 6. (**a**) Plot of the mean versus the standard deviation of the framboid size distribution of two wells. Dashed lines at the euxinic–anoxic boundary and the dysoxic–oxic boundary are from Wilkin et al. (1996) [11] and Chang et al. (2009) [45]; (**b**) plot of the mean versus the skewness of the framboid size distribution of two wells. The dashed line is from Wilkin et al. (1996) [11].

All 32 samples are located in the area representing euxinic conditions, except for 8 samples (nos. 1, 3, 4, 7, 8 and 11 of the JY1 well and nos. 5 and 6 of the X well) that are located in the area representing dysoxic conditions (Figure 6). No. 1, no. 3, no. 4 and no. 7; no. 8; and no. 11 of the JY1 well come from Long12, Long11-4 and Long11-3, respectively. No. 5 and no. 6 of the X well come from Long11-3 and Long11-4, respectively. All strata from the Wufeng Formation to the Long11-2 section are located in the euxinic area, and most of the samples from the Long13 to Long12 section are located in the anoxic–dysoxic area (Figure 6), which suggests that, from the Wufeng Formation to the Long12 sub-member, the redox conditions of the water column in the Long13 section changed from euxinic to anoxic–dysoxic.

Based on the statistics of the pyrite framboid size distribution from the Wufeng–Longmaxi shale, we reconstructed the redox condition change sequence from the Wufeng Formation to the Long12 sub-member (Figures 7 and 8).

The commercial shale gas-yielding strata from the Wufeng Formation to the Long11-4 section were deposited under dominant euxinic conditions, with dysoxic conditions occurring in the middle-upper part of Long13 and Long14. The Long12 sub-member is generally dominated by silty shale, and the silt laminations are relatively developed, with locally deposited carbonaceous shale. The Long12 sub-member is mainly an anoxic–dysoxic sedimentary environment, and the locality may be a euxinic environment. At the same time, the change trend in this environment is similar to the change in the TOC value (Figure 8).

Although the amount of silt in shale has increased since the Long13 section, the U/Th ratio is greatly affected by terrigenous clast, which causes the U/Th ratio to be greatly reduced, so it cannot be used. The other element ratios are less affected, and the use of trace element ratios in general can still more accurately determine the shale depositional environment (Figure 9).

Based on the analysis of trace element ratios (e.g., V/Cr, V/Sc, δU and V/(V + Ni)), it can be known that the Wufeng Formation–the lower part of the Long13 section is a euxinic environment, and the middle-upper part of the Long13–Long12 sub-member is a dysoxic sedimentary environment (Figure 9). This is consistent with the estimation of the Wufeng Long12 sedimentary environment by pyrite particle size distribution, which shows that it is accurate and reliable to use pyrite framboids to judge the sedimentary environment of the Wufeng–Longmaxi Formation shale.

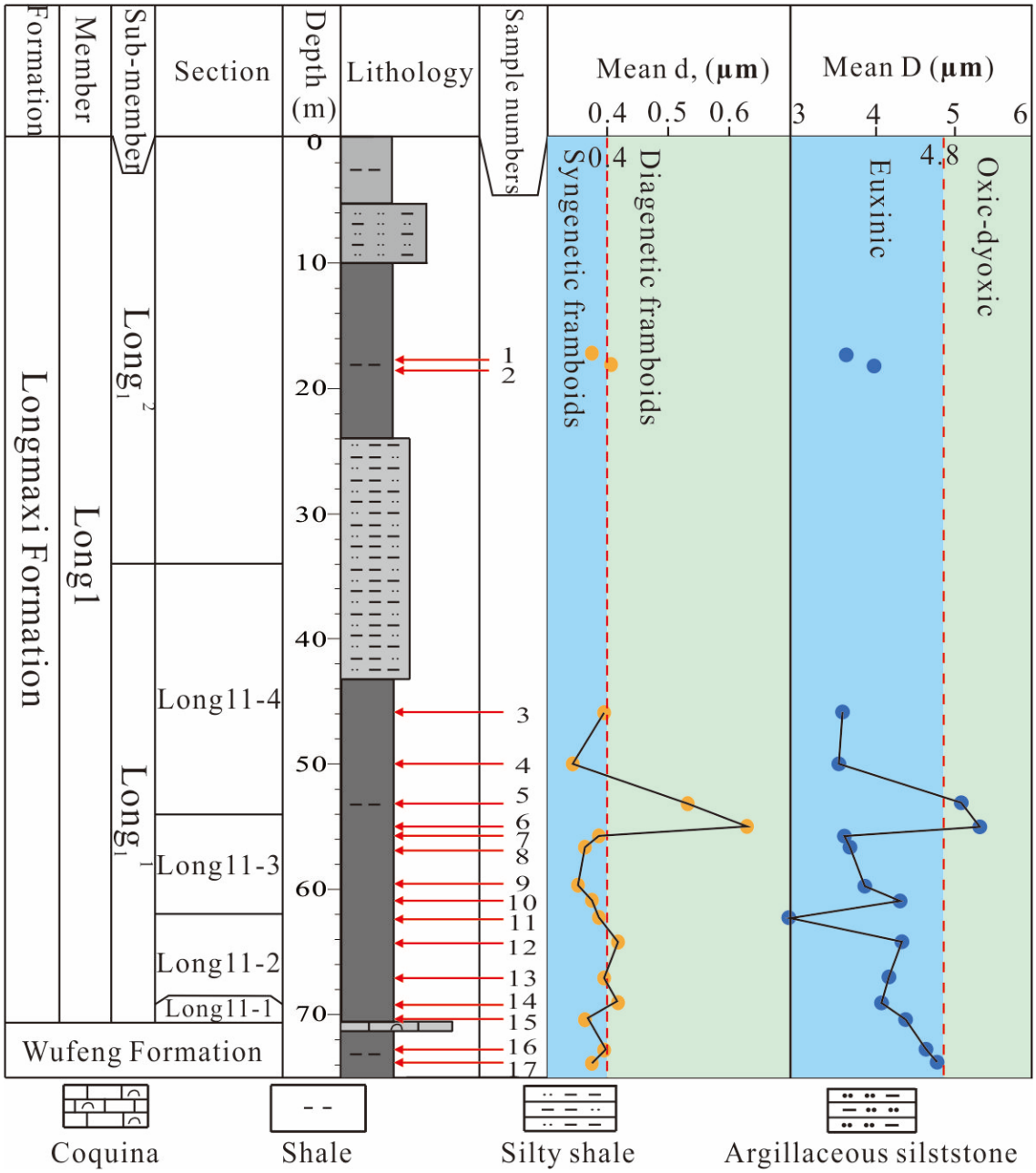

Figure 7. The mean, D, mean, d, and redox condition variations in the Wufeng–Longmaxi marine shale of the X well in the southeast Sichuan Basin.

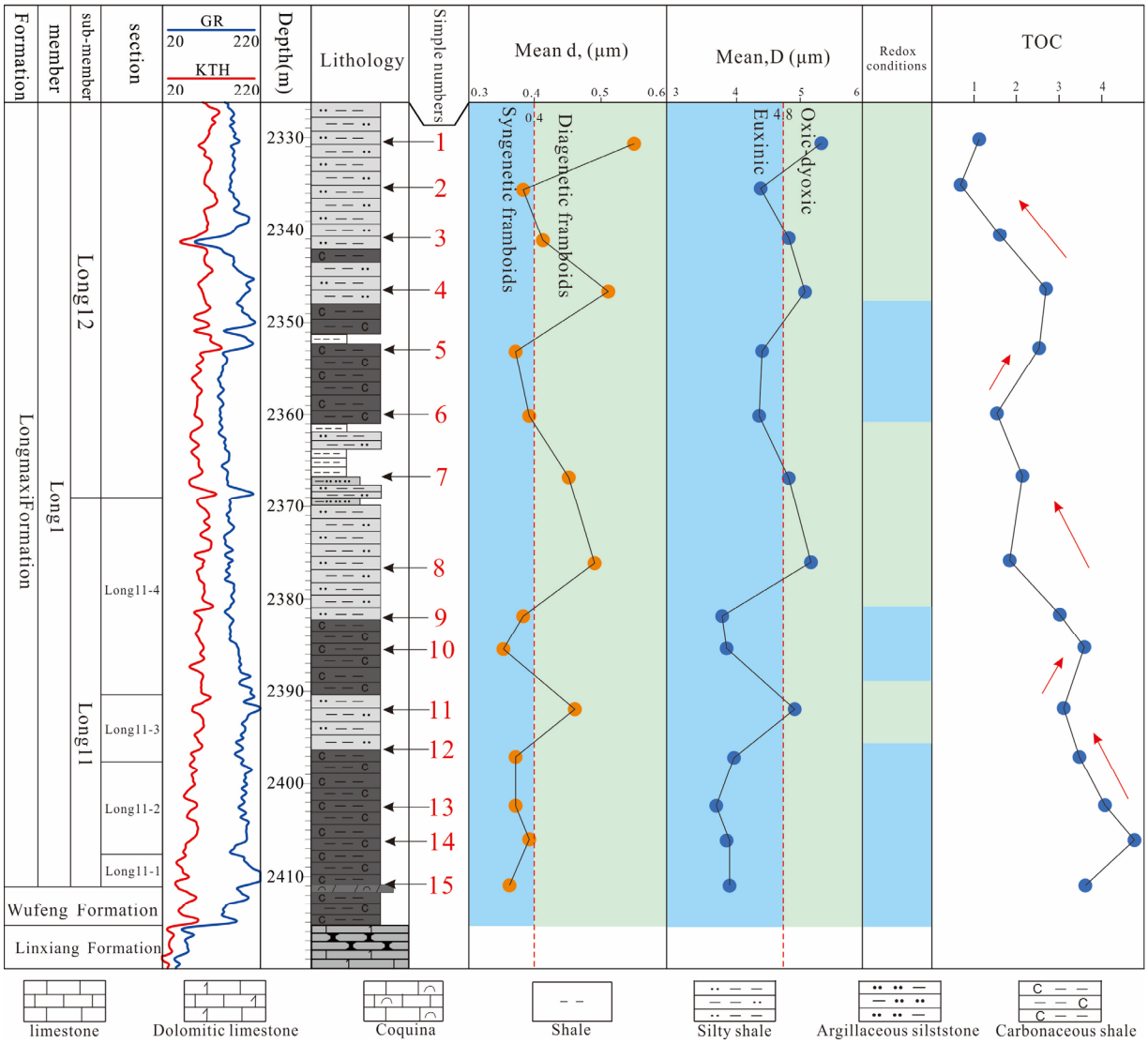

Figure 8. The mean, D, mean, d, redox condition variations and TOC of the Wufeng–Longmaxi marine shale of the JY1 well in the Jiaoshiba area, southeast Sichuan Basin.

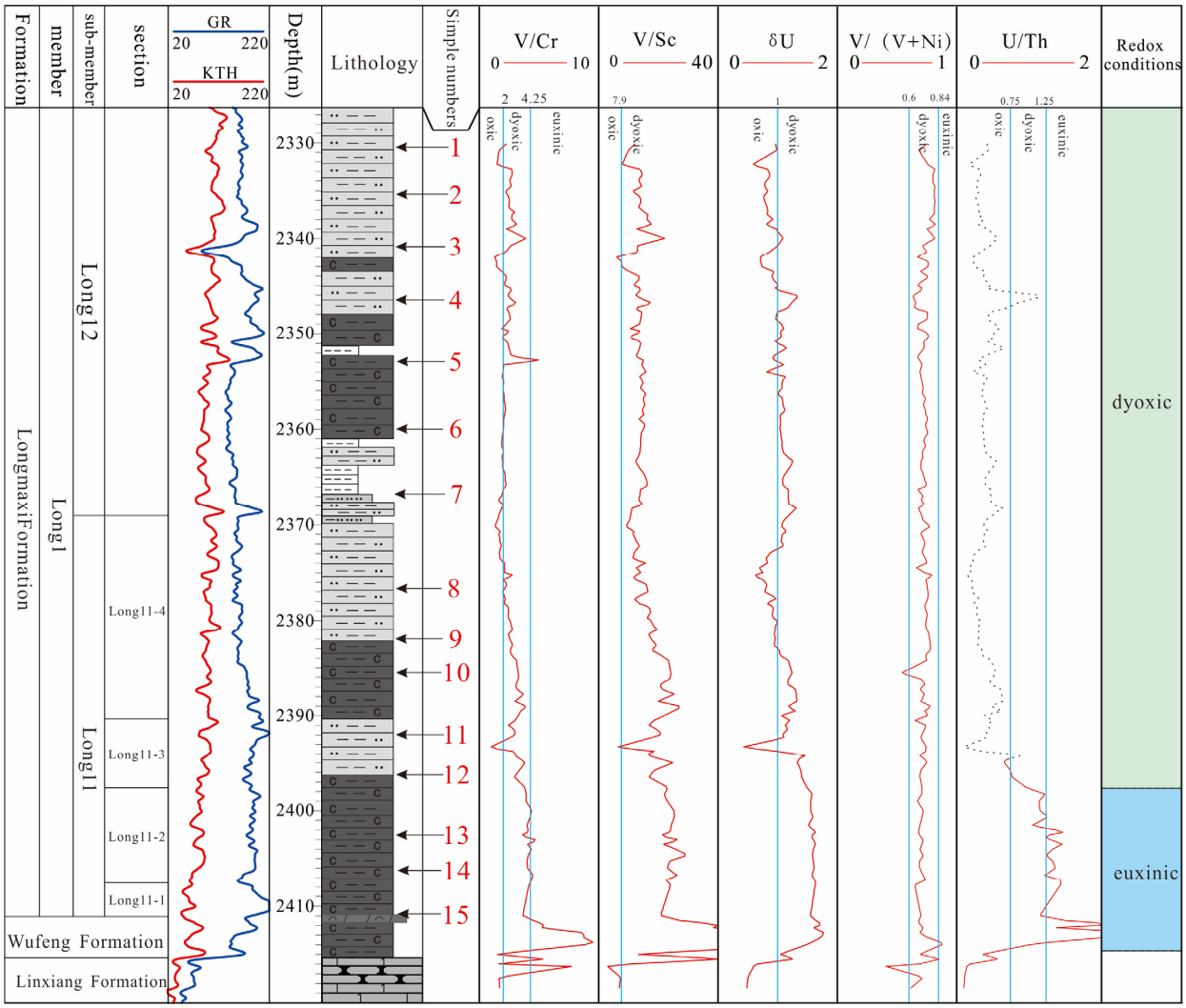

Figure 9. The redox condition variations in the Wufeng–Longmaxi marine shale of the JY1 well in the Jiaoshiba area, southeast Sichuan Basin.

5. Conclusions

Based on cores, FIB-SEM and statistical data of pyrite framboids, the pyrite characteristics and the environmental significance of the Lower Silurian Longmaxi marine shale in southeast Sichuan were analyzed in detail. The main conclusions are as follows:

1. Pyrite shows various occurrences in the drilling core, mainly occurring in the form of lamination with thicknesses ranging from 0.5 cm to 3 cm, and lenticular or pyrite nodules are discontinuously distributed with nodule sizes ranging from 0.5 cm × 2 cm to 1 cm × 3 cm.
2. At the micro-scale, an abundant occurrence of pyrite can be found in the Wufeng–Longmaxi marine shale. The pyrites in the Wufeng–Longmaxi shales mainly occur as three types: pyrite framboids, subhedral–euhedral pyrites and infilled pyrite framboids.
3. The statistics of pyrite framboids from all samples show that euxinic conditions dominated the Wufeng Formation to the lower part of the Long11-3 section, which is conducive to the preservation of organic matter. However, the middle-upper part of the Long13–Long12 sub-member is a dysoxic sedimentary environment. Through the judgment of pyrite in a sedimentary environment, it can be shown that high-quality shale development intervals are conducive to the exploration and development of shale gas in the later stage.

Author Contributions: Conceptualization, L.C., X.C. and X.T.; methodology, X.C.; software, X.C.; validation, L.C. and X.C.; formal analysis, X.C. and G.W.; investigation, X.C. and X.H.; resources, L.C. and X.H.; data curation, X.C. and G.W.; writing—original draft preparation, X.C.; writing—review and editing, L.C. and X.T.; visualization, X.C. and G.W.; supervision, L.C.; project administration, L.C.; funding acquisition, L.C. All authors have read and agreed to the published version of the manuscript.

Funding: This study was supported by the National Natural Science Foundation of China (NSFC) (No. 41602147) and Open Fund of State Key Laboratory of Oil and Gas Reservoir Geology and Exploitation (Southwest Petroleum University) (No. PLN1414).

Data Availability Statement: Data available on request due to restrictions e.g., privacy or ethical. The data presented in this study are available on request from the corresponding author. The data are not publicly available due to [a temporary secret of the project's needs].

Acknowledgments: We wish to thank PetroChina for providing the samples and some test data for this study.

Conflicts of Interest: The authors declare no conflict of interest.

References

1. David, R.; Luther, G.W. Chemistry of iron sulfides. *Chem. Rev.* **2007**, *107*, 514–562. [CrossRef]
2. Sweeney, R.E.; Kaplan, I.R. Pyrite framboid formation: Laboratory synthesis and marine sediments. *Econ. Geol.* **1973**, *68*, 618–634. [CrossRef]
3. Taylor, G.R. A mechanism for framboid formation as illustrated by a volcanic exhalative sediment. *Min. Depos.* **1982**, *17*, 23–36. [CrossRef]
4. Ohfuji, H.; Boyle, A.P.; Prior, D.J.; Richard, D. Structure of framboidal pyrite: An electron backscatter diffraction study. *Am. Mineral.* **2005**, *90*, 1693–1704. [CrossRef]
5. Wei, H.Y.; Wei, X.M.; Qiu, Z.; Song, H.Y.; Shi, G. Redox conditions across the G–L boundary in South China: Evidence from pyrite morphology and sulfur isotopic compositions. *Chem. Geol.* **2016**, *440*, 1–14. [CrossRef]
6. Liu, Z.Y.; Chen, D.X.; Zhang, J.C.; Lu, X.X.; Wang, Z.Y.; Liao, W.H.; Shi, X.B.; Tang, J.; Xie, G.J. Pyrite Morphology as an Indicator of Paleoredox Conditions and Shale Gas Content of the Longmaxi and Wufeng Shales in the Middle Yangtze Area, South China. *Minerals* **2019**, *9*, 428. [CrossRef]
7. Chu, F.Y.; Chen, L.R.; Shen, S.X.; Li, A.C.; Shi, X.F. Origin and environmental significance of authigenic pyrite from the south Yellow (Huanghai) Sea sediments. *Oceanoligica Limnol. Sin.* **1995**, *3*, 227–233. Available online: http://CNKI:SUN:HYFZ.0.1995-03-000 (accessed on 2 May 2022).
8. Grimes, S.T.; Davies, K.L.; Butler, I.B.; Brock, F.; Edwards, D.; Richard, D.; Briggs, D.E.G.; Parkes, R.J. Fossil Plants from the Eocene London Clay: The use of Pyrite textures to determine the mechanism of Pyritization. *J. Geol. Soc.* **2002**, *159*, 493–501. [CrossRef]
9. Wilkin, R.T.; Barnes, H.L. Pyrite formation by reactions of iron monosulfides with dissolved inorganic and organic sulfur species. *Geochim. Cosmochim. Acta* **1996**, *60*, 4167–4179. [CrossRef]
10. Butler, I.B.; Rickard, D. Framboidal pyrite formation via the oxidation of iron (II) monosulfide by hydrogen sulphide. *Geochim. Cosmochim. Acta* **2000**, *64*, 2665–2672. [CrossRef]
11. Wilkin, R.T.; Barnes, H.L.; Brantley, S.L. The size distribution of framboidal pyrite in modern sediments: An indicator of redox conditions. *Geochim. Cosmochim. Acta* **1996**, *60*, 3897–3912. [CrossRef]
12. Bottcher, M.E.; Lepland, A. Biogeochemistry of sulfur in a sediment core from the west–central Baltic Sea: Evidence from stable isotopes and pyrite textures. *J. Marine Syst.* **2000**, *25*, 299–312. [CrossRef]
13. Wilkin, R.T.; Arthur, M.A. Variations in pyrite texture, sulfur isotope composition, and iron systematics in the Black Sea: Evidence for Late Pleistocene to Holocene excursions of the O_2–H_2S redox transition. *Geochim. Cosmochim. Acta* **2001**, *65*, 1399–1416. [CrossRef]
14. Bond, D.; Wignall, P.B.; Racki, G. Extent and duration of marine anoxia during the Frasnian–Famennian (Late Devonian) mass extinction in Poland, Germany, Austria and France. *Geol. Mag.* **2004**, *141*, 173–193. [CrossRef]
15. David, R. How long does it take a pyrite framboid to form? *Earth Planet. Sci. Lett.* **2019**, *513*, 64–68. [CrossRef]
16. Tagliavento, W.; Lauridsen, B.W.; Stemmerik, L. Episodic dysoxia during Late Cretaceous cyclic chalk-marl deposition—Evidence from framboidal pyrite distribution in the upper Maastrichtian Rørdal Mb., Danish Basin. *Cretac. Res.* **2020**, *106*, 104223. [CrossRef]
17. Małgorzata, W.B.; Mariusz, R.; Leszek, M. Early Oligocene environment of the Central Paratethys revealed by biomarkers and pyrite framboids from the Tarcău and Vrancea Nappes (Eastern Outer Carpathians, Romania). *Mar. Pet. Geol.* **2021**, *128*, 105037. [CrossRef]
18. Wignall, P.B.; Newton, R. Pyrite framboid diameter as a measure of oxygen deficiency in ancient mudrocks. *Am. J. Sci.* **1998**, *298*, 537–552. [CrossRef]

19. Cai, Q.S.; Hu, M.Y.; Kane, O.I.; Li, M.T.; Zhang, B.M.; Hu, Z.G.; Deng, Q.J.; Xing, N. Cyclic variations in paleoenvironment and organic matter accumulation of the Upper Ordovician–Lower Silurian black shale in the Middle Yangtze Region, South China: Implications for tectonic setting, paleoclimate, and sea-level change. *Mar. Pet. Geol.* **2022**, *136*, 105477. [CrossRef]
20. Cai, Q.S.; Hu, M.Y.; Zhang, B.M.; Ngia, N.; Liu, A.; Liao, R.Q.; Kane, O.; Li, H.; Hu, Z.G.; Deng, Q.J.; et al. Source of silica and its implications for organic matter enrichment in the Upper Ordovician-Lower Silurian black shale in western Hubei Province, China: Insights from geochemical and petrological analysis. *Pet. Sci.* **2022**, *19*, 74–90. [CrossRef]
21. Yang, P.; Yu, Q.; Mou, C.L.; Wang, Z.J.; Liu, W.; Zhao, Z.; Liu, J.H.; Xiong, G.Q.; Deng, Q. Shale gas enrichment model and exploration implications in the mountainous complex structural area along the southwestern margin of the Sichuan Basin: A new shale gas area. *Nat. Gas Ind. B* **2021**, *8*, 431–442. [CrossRef]
22. Chen, L.; Lu, Y.C.; Jiang, S.; Li, J.Q.; Guo, T.L.; Luo, C. Heterogeneity of the Lower Silurian Longmaxi marine shale in the southeast Sichuan Basin of China. *Mar. Pet. Geol.* **2015**, *65*, 232–246. [CrossRef]
23. Guo, L.; Jia, C.C.; Du, W. Geochemistry of lower Silurian shale of Longmaxi Formation, southeastern Sichuan Basin, China: Implications for provenance and source weathering. *J. Cent. South Univ.* **2016**, *23*, 669–676. [CrossRef]
24. Ma, Y.Q.; Fan, M.J.; Lu, Y.C.; Guo, X.S.; Hu, H.Y.; Chen, L.; Wang, C.; Liu, X.C. Geochemistry and sedimentology of the Lower Silurian Longmaxi mudstone in southwestern China: Implications for depositional controls on organic matter accumulation. *Mar. Pet. Geol.* **2016**, *75*, 291–309. [CrossRef]
25. Wang, S.F.; Dong, D.Z.; Wang, Y.M.; Li, X.J.; Huang, J.L. Sedimentary geochemical proxies for paleoenvironment interpretation of organic–rich shale: A case study of the Lower Silurian Longmaxi Formation, Southern Sichuan Basin, China. *J. Nat. Gas Sci. Eng.* **2016**, *28*, 691–699. [CrossRef]
26. Shu, Y.; Lu, Y.C.; Chen, L.; Wang, C.; Zhang, B.Q. Factors influencing shale gas accumulation in the lower Silurian Longmaxi formation between the north and South Jiaoshiba area, Southeast Sichuan Basin, China. *Mar. Pet. Geol.* **2020**, *111*, 905–917. [CrossRef]
27. Rickard, D. Sedimentary pyrite framboid size-frequency distributions: A meta-analysis. *Palaeogeogr. Palaeoclimatol. Palaeoecol.* **2019**, *522*, 62–75. [CrossRef]
28. Nie, H.K.; Zhang, J.C. Shale gas reservoir distribution geological law, characteristics and suggestions. *J. Cent. South Univ.* **2010**, *41*, 700–708. [CrossRef]
29. Guo, T.L. Evaluation of Highly Thermally Mature Shale–Gas Reservoirs in Complex Structural Parts of the Sichuan Basin. *J. Earth Sci.-China* **2013**, *24*, 863–873. [CrossRef]
30. Chen, L.; Lu, Y.C.; Jiang, S.; Li, J.Q.; Guo, T.L.; Luo, C.; Xing, F.C. Sequence stratigraphy and its application in marine shale gas exploration: A case study of the Lower Silurian Longmaxi Formation in the Jiaoshiba shale gas field and its adjacent area in southeast Sichuan Basin, SW China. *J. Nat. Gas Sci. Eng.* **2015**, *27*, 410–423. [CrossRef]
31. Guo, X.S.; Hu, D.F.; Wen, Z.D.; Liu, R.B. Major factors controlling the accumulation and high productivity in marine shale gas in the Lower Paleozoic of Sichuan Basin and its periphery: A case study of the Wufeng–Longmaxi Formation of Jiaoshiba area. *Geol. China* **2014**, *41*, 893–901. [CrossRef]
32. Jiang, S.; Zhang, J.C.; Jiang, Z.Q.; Xu, Z.Y.; Cai, D.S.; Chen, L.; Wu, Y.; Zhou, D.S.; Jiang, Z.L.; Zhao, X.B.; et al. Geology, resource potentials and properties of emerging and potential China shale gas and shale oil plays. *Interpretation* **2015**, *3*, SJ1–SJ11. [CrossRef]
33. Jiang, S.; Tang, X.L.; Long, S.X.; McLennan, J.; Jiang, Z.L.; Jiang, Z.Q.; Xu, Z.Y.; Chen, L.; Xue, G.; Shi, X.; et al. Reservoir quality, gas accumulation and completion quality assessment of Silurian Longmaxi marine shale gas play in the Sichuan Basin, China. *J. Nat. Gas Sci. Eng.* **2017**, *39*, 203–215. [CrossRef]
34. Xiong, J.; Liu, X.; Liang, L. Experimental study on the pore structure characteristics of the Upper Ordovician Wufeng Formation shale in the southwest portion of the Sichuan Basin, China. *J. Nat. Gas Sci. Eng.* **2015**, *22*, 530–539. [CrossRef]
35. Xiong, J.; Liu, X.; Liang, L. Application of adsorption potential theory to methane adsorption on organic–rich shales at above critical temperature. *Environ. Earth-Sci.* **2018**, *77*, 99. [CrossRef]
36. Chen, X.; Xiao, C.X.; Chen, H.Y. Wufengian (Ashgillian) graptolite faunal differentiation and Anoxic environment in South China. *Acta Palaeontol. Sin.* **1987**, *26*, 326–344. [CrossRef]
37. Chen, X.; Rong, J.S.; Mitchell, C.E.; Harper, D.A.T.; Zhan, R.B.; Zhang, Y.D.; Li, R.Y.; Wang, Y. Late Ordovician to earliest Silurian graptolite and brachiopod biozonation from the Yangtze region, South China, with a global correlation. *Geol. Mag.* **2000**, *137*, 623–650. [CrossRef]
38. Chen, X.; Melchin, M.J.; Fan, J.X.; Mitchell, C.E. Ashgillian graptolite fauna of the Yangtze region and the biogeographical distribution of diversity in the latest Ordovician. *Bull. Soc. Géol. Fr.* **2003**, *174*, 141–148. [CrossRef]
39. Chen, X.; Fan, J.X.; Melchin, M.J.; Mitchell, C.E. Hirnantian (Latest Ordovician) graptolites from the upper Yangtze region, China. *Palaeontology* **2005**, *48*, 235–280. [CrossRef]
40. Chen, X.; Chen, L.; Tan, X.C.; Shu, J.; Wang, G.X. Impact of pyrite on shale gas enrichment—A case study of the Lower Silurian Longmaxi Formation in southeast Sichuan Basin. *Front. Earth Sci.* **2021**, *15*, 332–342. [CrossRef]
41. Liu, S.G.; Ma, W.X.; Jansa, L.B.; Huang, W.M.; Zeng, X.L.; Zhang, C.J. Characteristics of the shale gas reservoir rocks in the Lower Silurian Longmaxi Formation, East Sichuan basin, China. *Acta Petrol. Sin.* **2011**, *27*, 2239–2252. [CrossRef]
42. Wang, Y.M.; Dong, D.Z.; Li, J.Z.; Wang, S.J.; Li, X.J.; Wang, L.; Cheng, K.M.; Huang, J.L. Reservoir characteristics of shale gas in Longmaxi Formation of the Lower Silurian, southern Sichuan. *Acta Pet. Sin.* **2012**, *33*, 551–561. [CrossRef]

43. Bond, D.P.G.; Wignall, P.B. Pyrite framboid study of marine Permian–Triassic boundary sections: A Complex anoxic event and its relationship to contemporaneous mass extinction. *Geo. Soc. Am. Bull.* **2010**, *122*, 1265–1279. [CrossRef]
44. Wignall, P.B.; Bond, D.P.G.; Kuwahara, K.; Kakuwa, Y.; Newton, R.J.; Poulton, S.W. An 80 million year oceanic redox history from Permian to Jurassic Pelagic sediments of the Mino–Tamba terrane, SW Japan and the origin of four mass extinctions. *Glob. Planet Chang.* **2010**, *71*, 109–123. [CrossRef]
45. Chang, H.J.; Chu, X.L.; Feng, L.J.; Huang, J. Framboidal pyrites in cherts of the Laobao Formation, South China: Evidence for anoxic deep ocean in the terminal Ediacaran. *Acta Petrol. Sin.* **2009**, *25*, 1001–1007. [CrossRef]